

Photoreduction of CO₂ using sol–gel derived titania and titania-supported copper catalysts

I-Hsiang Tseng, Wan-Chen Chang, Jeffrey C.S. Wu*

Department of Chemical Engineering, National Taiwan University, Taipei 10617, Taiwan, ROC

Received 28 August 2001; received in revised form 16 November 2001; accepted 19 November 2001

Abstract

Carbon dioxide was photocatalytically reduced to produce methanol in an aqueous solution using 254 nm UV irradiation. Titania and Cu-loaded titania were synthesized by an improved sol–gel method using a homogeneous hydrolysis technique. The grain size of TiO₂ and Cu/TiO₂ were uniform and average diameters were approximately 20 nm. Photocatalytic reduction was conducted in a quartz reactor with a UV lamp irradiating at the center. XPS analysis reveals that Cu 2p_{3/2} is 933.4 eV indicating primary Cu₂O species on the TiO₂ supports. EDX and XPS revealed that most copper clusters were on the TiO₂ surface. The optimum amount of copper loading was 2.0 wt.% for the highest dispersion among catalysts. The methanol yield of 2.0 wt.% Cu/TiO₂ was 118 μmol/g following 6 h of UV illumination. The yield was much higher than those of sol–gel TiO₂ and Degussa P25, whose yields were 4.7 and 38.2 μmol/g, respectively. The methanol yield reached a steady-state 250 μmol/g after 20 h of irradiation. Experimental results indicated that the methanol yield was significantly increased by adding NaOH. The caustic solution dissolved more CO₂ than did pure water. In addition, the OH[−] in aqueous solution also served as a strong hole scavenger. The redistribution of the electric charge and the Schottky barrier of Cu and TiO₂ facilitates electron trapping via supported Cu. The photocatalytic efficiency of Cu/TiO₂ was markedly increased because of the lowering the re-combination probability for hole–electron pairs. The highest quantum and energy efficiencies achieved were 10 and 2.5%, respectively. © 2002 Elsevier Science B.V. All rights reserved.

Keywords: Photocatalytic reduction; Carbon dioxide; Titanium dioxide; Sol–gel; Copper

1. Introduction

Greenhouse gases such as CO₂, CH₄ and CFCs are the primary causes of global warming. The atmospheric concentration of CO₂ has recently increased owing to human activity, further accelerating the greenhouse effect. In response, the Kyoto Protocol of the United Nations Framework Convention on Climate Change mandated a return of CO₂ emission levels to those of 1990. Although the remediation of CO₂ can

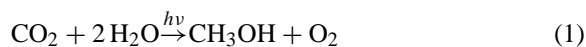
be physically stored or chemically transformed, storage overcomes the problem only temporarily. To solve the CO₂ problem permanently requires transforming CO₂ into another useful or non-toxic compounds. Upgrading CO₂ to reusable hydrocarbon resources would benefit humans and the environment.

The energy grade of CO₂ is low from a thermodynamic perspective, accounting for why any transformation to hydrocarbon requires energy infusion. The energy source should be provided without producing more CO₂, such as solar energy. Plants use solar energy to perform natural photosynthesis, but the energy transformation is low at the cost of supporting their lives. Even under the optimal artificial

* Corresponding author. Tel.: +886-22363-1994;
fax: +886-23632-3040.
E-mail address: cswu@ccms.ntu.edu.tw (J.C.S. Wu).

conditions, energy efficiency can only reach about 10% in macroalga under full sunlight [1]. Solar energy is the Earth's ultimate power supply. All energy forms except geothermal or nuclear, such as fossil fuel, bio-material, hydropower and wind are various kinds of transformation from sun. Consequently, the photoreduction of CO₂ is particularly interesting, and achieving a high efficiency for this reaction is highly desired. The ultimate goal is to demonstrate that artificial photosynthesis may be implemented via the photoreduction of CO₂ to produce hydrocarbons, such as methanol or methane. That is, solar energy is transformed and stored as chemical energy. Moreover, methanol is the most promising photo-reduced product of carbon dioxide because it can be transformed into other useful chemicals using conventional chemical technologies, or easily transported and used as fuel-like renewable energy.

Many researchers have shown that CO₂ can be reduced in water vapor or solvent by photocatalysts such as TiO₂ and ZnS [2,3]. From a thermodynamic perspective, transforming 1 mol of CO₂ into methanol requires 228 kJ. Six electrons are required to convert the C⁴⁺ of CO₂ to the C²⁻ of methanol. Eq. (1) describes the overall reaction.



The efficient photoreduction of CO₂ with H₂O is one of the most challenging tasks of environmental catalysts. As well known, titania is a photoexcited catalyst. The bandgap of anatase form TiO₂ is 3.2 eV, making it a perfect candidate for UV illumination. Titania-supported copper plays a crucial role for promoting the reduction of CO₂ [4]. This work aims to improve the photoreduction efficiency by using supported Cu-titania catalysts prepared by an improved sol-gel technique. Other variables important in photoreducing CO₂, such as CO₂ pressure, concentration of catalyst and copper loading are investigated. The activity of a photocatalytic reaction is usually difficult to compare between research reports. Although the photoactivity can usually be presented by product yield, e.g. μmol/(g-cat s) or μmol/g-cat, the yield can be changed substantially under different experimental conditions such as UV wavelength, UV intensity, additives of reaction media and reactor configuration. In this study, in addition to product yield, quantum and

energy efficiencies are proposed and presented for the photoactivity of our system.

2. Experimental

2.1. Preparation and characterization of catalysts

Catalysts were prepared via the sol-gel route illustrated in Fig. 1. The precursor was titanium(IV) butoxide (Ti(OC₄H₉)₄, 97% in *n*-butanol), as purchased from Aldrich (USA). The hydrolysis process was performed in a glove box maintained at a relative humidity under 25% by purging with tank nitrogen. To avoid rapid precipitation during polycondensation and the formation of unstable colloidal sols, the hydrolyzing water was homogeneously released by the esterification of butanol and acetic acid [5]. The basic aim was to provide the appropriate stoichiometric quantity of water to hydrolyze titanium butoxide during hydrolysis. A typical batch contained 0.02 mol titanium butoxide, 0.08 mol anhydrous butanol (minimum 99.8%) and 0.08 mol glacial acetic acid (minimum 99.7%). The clear solution was stirred for 8 h

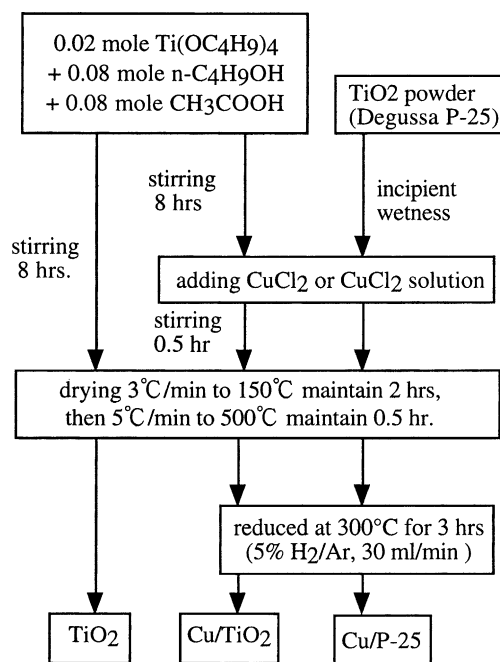


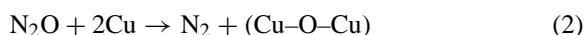
Fig. 1. The procedure of catalysts preparation.

at which time the pH value became stabilized. The final pH value of the solution approached 3.56. The transparent sol was dried from room temperature to 150 °C in an oven, then transferred to a furnace and calcined at 500 °C to burn off hydrocarbons. The sample was crushed into powder in a mortar. The JRC-2 and P25 titania powders were obtained from Fuji Titan (Japan) and Degussa (Germany), respectively, for comparison. Copper-loaded titania (Cu/TiO₂) and P25 (Cu/P25) were impregnated by adding CuCl₂ during the sol–gel process and incipient wetness method, respectively. Following calcination similar to that of TiO₂, Cu-loaded titania was reduced under a flow of 5% H₂/Ar mixture at 300 °C for 3 h.

The specific surface area and pore size distribution of catalysts were measured by N₂ adsorption in a Micromeritics ASAP 2000. A diffusive reflective UV–VIS spectrophotometer (Hitachi U-3410) was employed to measure the UV–VIS absorption and estimate the bandgap of the catalysts. The particle size distribution in aqueous solution was obtained using a Coulter LS230 particle size analyzer. Transmission electron microscopy (TEM) and scanning electron microscopy with energy dispersive X-ray spectrometer (SEM-EDX, Philips XL30, EDAX DX4) were used to observe the morphology of catalysts and estimate the elemental ratio. The crystalline phase was identified by X-ray diffraction (MAC MO3XHF). The chemical status and shift of the catalyst surface were analyzed by X-ray photoelectron spectroscopy (XPS). XPS measurements were taken on a VG Microtech MT500 spectrometer, operated with a constant pass energy of 50 eV and with Mg K α radiation as the excitation source ($h\nu = 1253.6$ eV). The catalyst was pressed into a pellet, and then adhered on sample holder by carbon tape. Oxygen (1 s, 530.7 eV for TiO₂) [6] and carbon (1 s, 284.5 eV) were taken as internal standards for binding energy calibration. The fluorescence spectra of catalysts were measured by a Jasco FP-777 fluorescence spectrophotometer at an excitation wavelength of 370 nm.

The copper dispersion of Cu/TiO₂ was measured using the method of Chang et al. [7]. The Cu/TiO₂ catalyst was reduced in a 5% H₂/Ar stream at 300 °C for 3 h. The catalyst was purged and cooled to 80 °C in Ar, and the oxidation was then performed using N₂O at that temperature. Only surface copper was selectively oxidized by N₂O when the oxidation temperature was

under less than 100 °C. The decomposition of N₂O on the Cu surface generated the chemisorbed oxygen atoms as shown in Eq. (2) [8]. Following oxidation, the catalyst was again purged in Ar and cooled to 25 °C. Hydrogen temperature programmed reduction (TPR) was performed from 25 to 400 °C at 10 °C/min in a 5% H₂/Ar stream. The consumption of H₂ was measured from TPR and the dispersion of copper was calculated.



2.2. Photocatalytic reaction

Fig. 2 schematically illustrates the reactor system. The system was illuminated by an 8 W Hg lamp with a peak light intensity at 254 nm in the center of the quartz reactor. The entire system was shielded by a metal case during the reaction to prevent interference from outside light. Catalyst powder (0.15–0.6 g) was suspended in 300 ml of 0.2 N NaOH aqueous solutions for typical batches. Supercritical-fluid grade CO₂ was purchased from Air Products (USA) to avoid any hydrocarbon contamination. It was certified maximum hydrocarbons less than 20 ppb. CO₂ was bubbled through the reactor for at least 30 min to purge air and to saturate the solution. The reactor was tightly closed during the reaction, and the CO₂ pressure was maintained in the range of 101.3–135.6 kPa. A magnetic stirrer agitated the catalyst-suspended solution at the

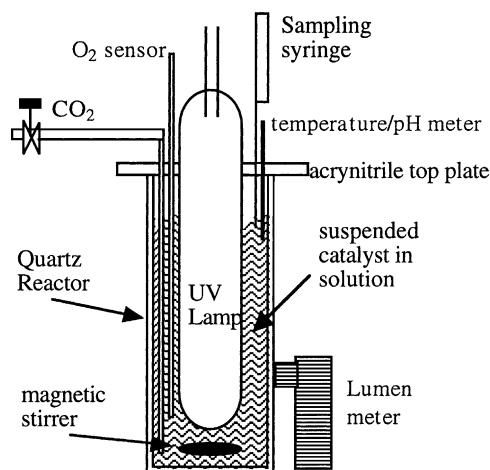


Fig. 2. Schematic of photocatalytic reaction.

bottom to prevent sedimentation of the catalyst. The steady-state temperature of the solution rose to almost 50 °C during illumination.

The release of O₂ during the reaction would constitute direct evidence of CO₂ photoreduction (Eq. (1)). An oxygen sensor (Mettler Toledo InPro[®] 6000 series) was placed in the reactor to monitor the concentration of dissolved O₂ during the photoreduction. The sensor was calibrated using the dual point mode before measuring O₂ concentration. The O₂ sensor was inserted into oxygen-free gel until the “ready” sign was on, to fix the zero point. Then, the sensor was put into O₂-saturated solution, until “ready” and the value was attuned to a verified concentration (8.2 ppm, 25 °C). A needle-type probe was inserted in the reactor to extract samples. The liquid sample (<0.5 ml) was collected in a vial wrapped in aluminum foil to reduce interference from the indoor fluorescent light before analysis. After the catalyst’s sedimentation, 1–10 µl liquid sample was withdrawn and analyzed in a GC/FID equipped with a 3 m long Porapak Q column. Analysis results indicated that methanol was the dominant hydrocarbon. Formic acid, formaldehyde and ethanol were detected from some catalytic reactions, in amounts much less than that of methanol.

An UVC probe (Oriol instrument, Goldilux model 70239) was attached on the outer wall of the quartz reactor, and the energy flux (µW/cm²) was indicated by a lumen meter (Oriol instrument, Goldilux model 70235) connected to the probe. The photon flux was obtained by dividing the energy flux by the energy of a photon with a wavelength of 254 nm. The energy flux was first measured for the reactor filled with water only. The energy flux was then measured for the reactor containing the catalyst and CO₂ during the reaction. The difference between those energy fluxes was the photo energy absorbed in photoreduction.

Blank reactions were conducted to ensure that hydrocarbon production was due to the photoreduction of CO₂, and to eliminate surrounding interference. One blank was UV-illuminated without the catalyst, and another was in the dark with the catalyst and CO₂ under the same experimental conditions. An additional blank test was UV-illuminated with the catalyst filling N₂ rather than CO₂. No hydrocarbon was detected in the above three blank tests.

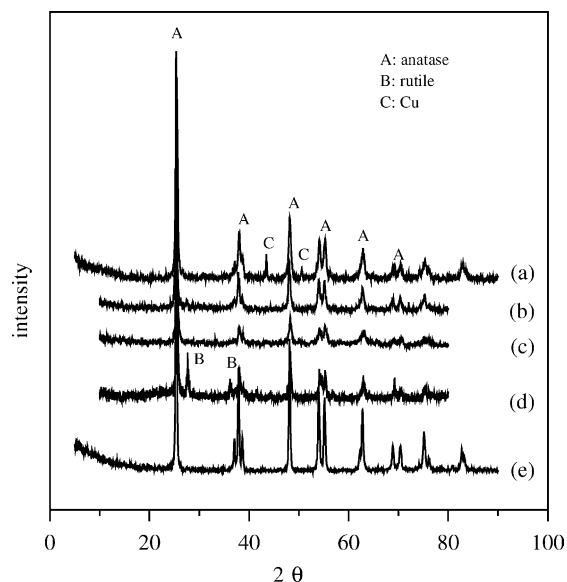


Fig. 3. XRD spectra of TiO₂ and Cu/TiO₂. (a) 6.7 wt.% Cu/ TiO₂; (b) 2.0 wt.% Cu/ TiO₂; (c) TiO₂; (d) P25; (e) JRC-2.

3. Results and discussion

3.1. Characteristics of catalysts

The XRD spectra in Fig. 3 verified the anatase phase of JRC-2, P25, TiO₂ and Cu/TiO₂. A previous investigation has indicated that anatase TiO₂ is the most active phase for photocatalytic reaction [9]. Two small Cu diffraction peaks appeared near $2\theta = 43.3$ and 52° on 6.7 wt.% Cu/TiO₂. No Cu peak was observed on 2.0 wt.% Cu/TiO₂, perhaps due to the slight Cu loading or the extremely small Cu clusters. The grain sizes of all sol–gel derived TiO₂ were nearly 20 nm, as calculated from the Scherrer equation. The particle sizes were consistent with the TEM observation displayed in Fig. 4. As shown in Fig. 4(a), the particles of sol–gel derived TiO₂ were uniform and the diameter was between 10 and 25 nm. Fig. 4(b) reveals that copper clusters were well dispersed on the surface of TiO₂. Copper clusters were expected to be present on the surface of the TiO₂ particle because the CuCl₂ was added after hydrolysis of titanium butoxide during the preparation (Fig. 1). Zhang et. al. suggested that pure TiO₂ grain sizes with a diameter ranging from 11 to 21 nm were of a size that maximized photocatalytic

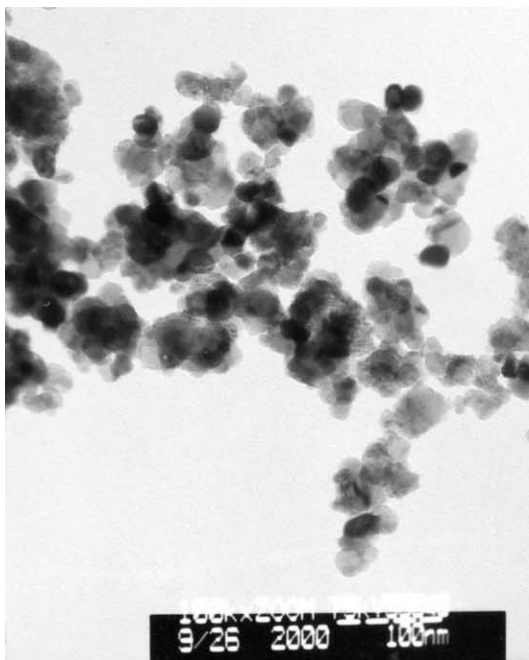
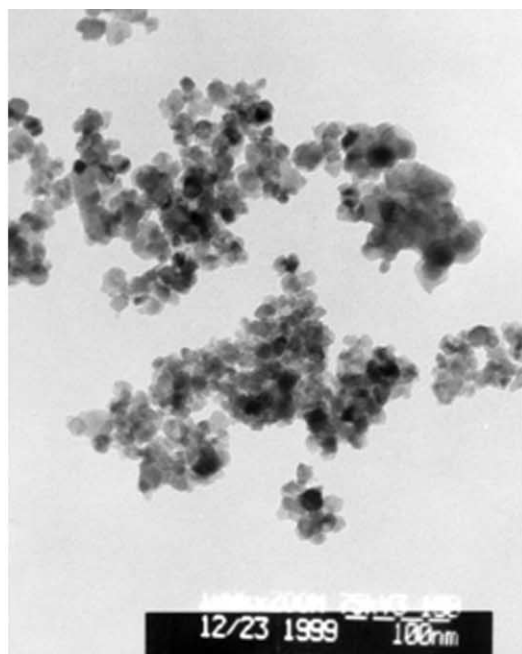


Fig. 4. TEM photographs (a) TiO_2 , (b) 3.3 wt.% Cu/TiO_2 .

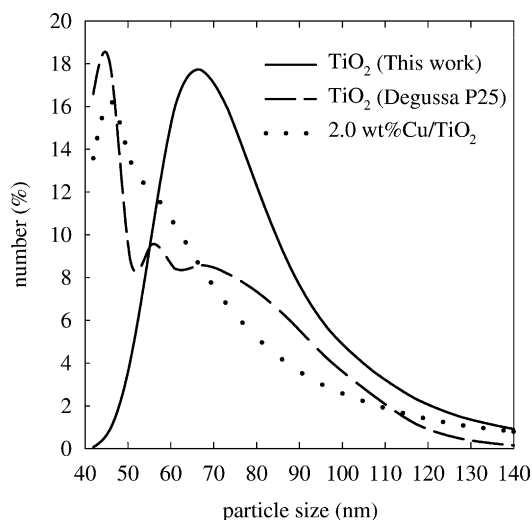


Fig. 5. The particle size distributions of P25, TiO_2 and Cu/TiO_2 .

efficiency [10]. When the particle size was less than 5–10 nm, the surface recombination of electron–hole pairs becomes significant, resulting in low photocatalytic efficiency. Fig. 5 shows the actual particle size distributions of catalysts in an aqueous suspension. For TiO_2 and 2 wt.% Cu/TiO_2 , the median particle sizes were near 70 and 50 nm, respectively. P25 exhibited two modes of particle size distribution, near 45 and 75 nm.

The bandgap can be estimated by extrapolating the rising portion of the UV spectrum to the abscissa at zero absorption [11]. Table 1 summarizes the properties of the catalysts. The bandgaps of JRC-2 and

Table 1
The properties of catalysts

Catalyst	Surface area (m^2/g)	Crystallize size ^a (nm)	Bandgap ^b (eV)
TiO_2 (this work)	63	18	2.95
Degussa P25	50 ^c	21	3.47
JRC-2	16 ^c	42	3.27
0.6% Cu/TiO_2	34	—	—
1.0% Cu/TiO_2	40	20	2.99
2.0% Cu/TiO_2	28	20	2.99
3.3% Cu/TiO_2	26	20	2.92
6.0% Cu/TiO_2	—	—	2.86
6.7% Cu/TiO_2	28	17	3.05

^a Estimated from FWHM of XRD by Scherrer equation.

^b Estimated from UV–VIS spectra.

^c From manufacturer.

Table 2

The element molar ratio of catalysts calculated from XPS and EDX analysis

Catalyst	Cu/Ti		
	Bulk	EDX	XPS
0.6 wt.% Cu/TiO ₂	0.007	0.013	—
1.0 wt.% Cu/TiO ₂	0.012	—	0.063
2.0 wt.% Cu/TiO ₂	0.02	0.035	0.119
3.3 wt.% Cu/TiO ₂	0.04	0.053	0.138
6.7 wt.% Cu/TiO ₂	0.09	0.091	0.165

P25 are 3.27 and 3.47 eV, respectively, while those of sol-gel TiO₂ and Cu/TiO₂ are nearby 3.00 eV. Notably, the bandgap is governed by the crystalline structure and the defects in the TiO₂ network. A related investigation suggested that small bandgaps were caused by the stoichiometric deficiency of Ti/O from the sol-gel processes [11]. The specific surface area of sol-gel derived catalysts ranged from 25 to 63 m²/g. The specific surface area of sol-gel TiO₂ was larger than that of commercial JRC-2 or P25.

Table 2 lists the elemental ratio of Cu/Ti estimated from XPS and EDX. The bulk ratio of Cu/Ti was the molar ratio of Cu and Ti in the sol-gel preparation (Fig. 1). The discrepancy between the Cu/Ti ratio obtained by EDX and XPS indicated that most Cu was on the surface of the TiO₂ support. The source of these two kinds of probes, X-ray and electron, with different incident energies, 50 eV and 15 keV, indicates that elements were detected with different depths, ~10 nm and ~1 μm, from the surface [12]. Accordingly, the quantitative results of XPS show the outmost surface of catalyst, while those of EDX give the deep structural layers and represent near bulk property.

Fig. 6 displays the XPS spectra of TiO₂, P25, JRC-2 and 2 wt.% Cu/TiO₂. The binding energies of Ti 2p_{3/2} and 2p_{1/2} of 2 wt.% Cu/TiO₂ are the same as those of pure titania at 459.4 and 465.3 eV, respectively, indicating the integrity of the TiO₂ structure, which was not modified by copper impregnation. Fig. 7 shows the XPS spectra of the hydrogen-reduced Cu/TiO₂ catalysts. The binding energies of Cu 2p_{3/2} and 2p_{1/2} were 933.4 and 954.3 eV, respectively. The shapes of the XPS spectra reveal that the copper species on TiO₂ are major Cu₂O and minor Cu⁰ [13].

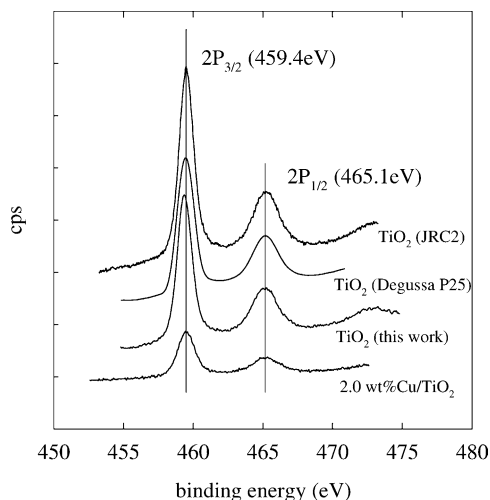


Fig. 6. XPS spectra of Ti2p of catalysts.

3.2. The photocatalytic reduction of CO₂

Fig. 8 shows the dependence of methanol formation on illumination time. Various yields of methanol were obtained in a period depending on the catalysts. In all cases, the concentration of methanol was too small to be measured by GC for nearly initial 180 min. The formation of methanol was found much

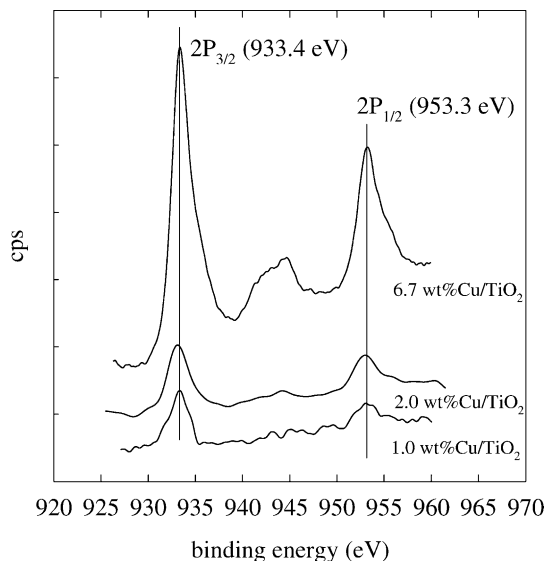


Fig. 7. XPS spectra of Cu2p of catalysts.

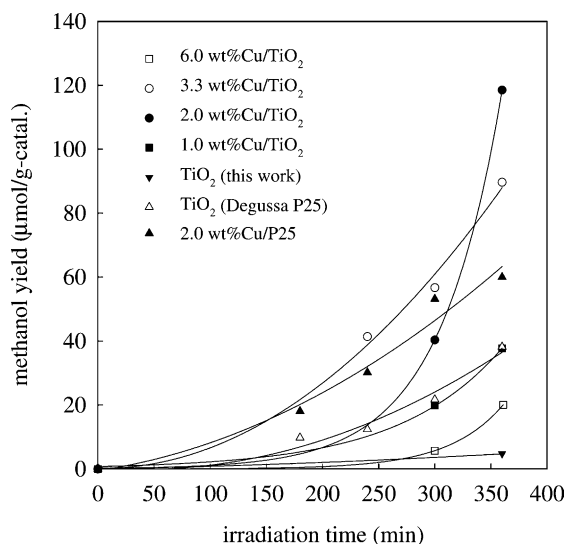


Fig. 8. Time dependence on the methanol yields of various catalysts.

more effective on supported Cu-titania catalyst [14]. Methane, formic acid and other hydrocarbons might have been generated, but in quantities too low to be detected. The results showed that the sol-gel derived Cu/TiO₂ outperformed P25, JRC-2, and 2 wt.% Cu/P25. Table 3 summarizes the methanol yields of various catalysts under 6 h irradiation. The presence of copper plays an important role, while specific surface area is obviously not a main factor in photocatalytic reactions [15].

Contact between TiO₂ and metal generally involves a redistribution of electric charge. In the presence of copper clusters, electrons are enriched owing to the alignment of Fermi levels of the metal and the semiconductor, that is the Schottky barrier [9]. Copper then serves as an electron trapper and prohibits the recombination of hole and electron. In addition, the rapid transfer of excited electrons to the copper cluster enhances the separation of holes and electrons [4], significantly promoting photoefficiency. The formation of methanol was more efficient than that of other hydrocarbons in the presence of supported Cu⁺ on TiO₂ from the CO₂ and H₂O system [14].

Fig. 9 presents the fluorescence spectra of P25, Cu/P25 and 2 wt.% Cu/TiO₂. The fluorescence intensity of Cu/P25 is much less than that of P25; and 2 wt.% Cu/TiO₂ gives an even lower intensity. The fluorescence of titania is caused by the recombination of electrons and holes [16]. The decline in fluorescence intensity is due to the reduced number of recombination sites on the TiO₂ surface. Fewer recombination sites on the surface lead to slower recombination of electrons and holes, thus a higher photocatalytic activity [17]. The copper-loaded titania effectively provides the electron traps and gives lower fluorescence intensity resulting in higher methanol yield.

Quantum efficiency is an essential factor to evaluate a photoexcited reaction, especially in solar energy utilization. Eq. (3) is proposed to determine the

Table 3

The methanol yield, energy efficiency (Φ_E), quantum efficiency (Φ_Q) and turnover frequency (for Cu site) of catalysts

Catalyst	6 h methanol yield ($\mu\text{mol/g catalyst}$)	Φ_E (%)	Φ_Q (%)	TOF (1/s)
TiO ₂	4.7	0.09	0.42	–
Degussa P25	38.2	0.81	3.41	–
JRC-2	3.4	0.07	0.27	–
2.0% Cu/P25	60.0	1.27	5.35	21
0.6% Cu/TiO ₂	37.7	0.79	3.16	58
1.0% Cu/TiO ₂	72.9	1.54	6.06	–
2.0% Cu/TiO ₂	118.5	2.50	10.02	40
3.3% Cu/TiO ₂	89.7	1.89	7.57	23
6.0% Cu/TiO ₂	20.0	0.79	1.67	7

Photon flux absorbed by catalyst = (measured photon flux without catalyst) – (measured photon flux with catalyst in reactor) = $\sim 138 \mu\text{W}/\text{cm}^2$. Outer surface area of reactor = 346.4 cm^2 . Each photon energy = $hc/\lambda = (6.6262 \times 10^{-34})(3 \times 10^8)/(2.54 \times 10^{-7}) = 7.826 \times 10^{-19} \text{ J}$. Total photons absorbed by catalyst in reactor = absorbed photon flux ($\mu\text{W}/\text{cm}^2$) \times outer surface area of reactor, (cm^2) \times radiation time (s)/each photon energy, (J)/ $6.02 \times 10^{23} = \sim 2189 \mu\text{mol}$.

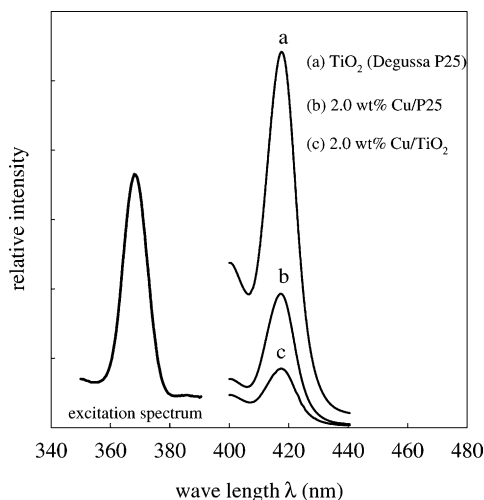


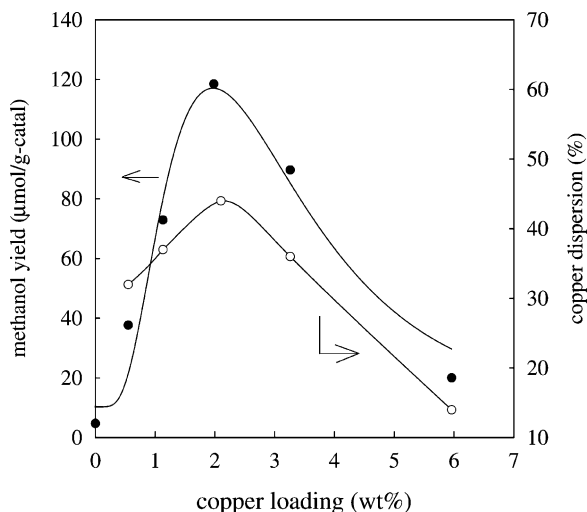
Fig. 9. The fluorescence spectra of catalysts.

quantum efficiency. Six moles of electrons are required to produce 1 mol of methanol from CO_2 (Eq. (1)). All methanol yields of catalysts were compared at 6 h of UV illumination. The total moles of photons were calculated from the 6 h period of photon flux. The energy efficiency (Eq. (4)) evaluates the transformation of the photon's energy into chemical energy. Theoretically, the chemical energy is the formation of methanol from CO_2 and H_2O . The equation is the reverse of Eq. (1), so the chemical energy is equal to the heat of methanol combustion. The photon energy is the radiation energy absorbed by the catalyst, and is measured by the lumen meter. Table 3 lists the calculated quantum and energy efficiencies. The highest quantum and energy efficiencies achieved 10 and 2.5%, respectively, on the 2.0 wt.% Cu/TiO_2 catalyst.

$$\text{quantum efficiency (\%)} = \frac{6 \times \text{moles of methanol yield}}{\text{moles of UV photon absorbed by catalyst}} \times 100 \quad (3)$$

$$\text{energy efficiency (\%)} = \frac{\text{heat of combustion} \times \text{moles of methanol yield}}{\text{radiation energy of UV absorbed by catalyst}} \times 100 \quad (4)$$

The effects of Cu loading and dispersion on methanol yields are shown in Fig. 10. The methanol yields increase with Cu loading, but then decrease when the Cu loading exceeds 2 wt.%. The Cu dispersions of Cu/TiO_2 increased slightly to 40% for Cu loading below 2 wt.%, then decreased with further Cu loading. The turnover frequency (TOF) of Cu/TiO_2

Fig. 10. Effect of Cu loading amount on copper dispersion and methanol yield under 6 h UV irradiation. (CO_2 pressure: 125 kPa).

catalyst can be estimated if we assume that entire photoreduction occurs on Cu active sites. Table 3 lists the TOFs of Cu/TiO_2 catalysts for known Cu dispersion. The TOF of 0.6 wt.% Cu/TiO_2 catalysts gave the highest value near 58, and TOFs decrease with increasing Cu loadings. Obviously, more Cu loading can increase methanol yield because of the amount of active sites. However, the photoactivity (TOF) of each Cu site declines with more Cu loading on TiO_2 surface. Therefore, catalysts with more than 2 wt.% Cu loading cannot further increase the methanol yield due to the decreasing TOF. Furthermore, excess Cu loading can mask the TiO_2 surface, reducing the photoexciting capacity of TiO_2 . There exists an optimum amount of copper loading, around

2 wt.% under the experimental conditions of this work.

The catalyst, 2 wt.% Cu/TiO_2 , was chosen for further studying the long-term reaction and the influence of experimental conditions. Fig. 11 shows the time dependency of methanol yields with long irradiation periods of up to 35 h. The reactions were

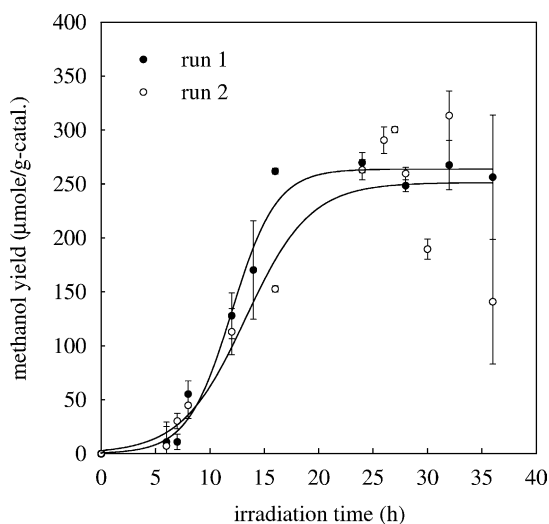


Fig. 11. Methanol yields of two 2.0 wt.% Cu/TiO₂ catalysts under long-term UV irradiation (CO₂ pressure: 125 kPa).

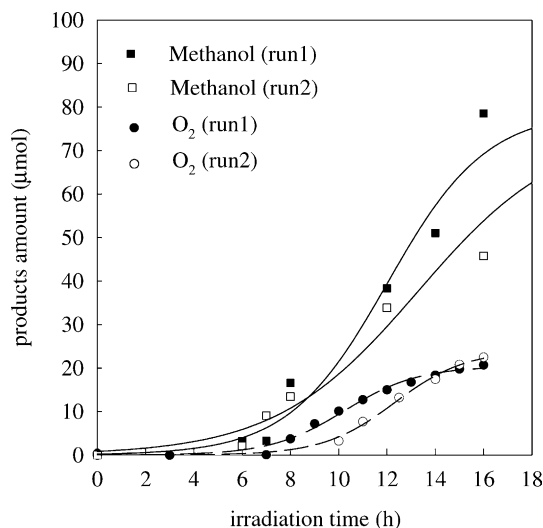


Fig. 12. The dissolved O₂ of two 2.0 wt.% Cu/TiO₂ catalysts during reaction.

repeated twice to confirm the reproducibility and consistency using two different batches of catalysts with the same Cu loading. A steady-state methanol yield was around 250 $\mu\text{mol/g}$ following nearly 20 h of irradiation. Halmann suggested that the oxidation of hydrocarbons could occur on the anodic site on TiO₂ particles [18]. The rate of methanol re-oxidation eventually caught up with that of methanol generation from CO₂ reduction, thus reaching a steady-state methanol concentration. Another explanation of limited yields involves the deactivation of catalysts due to the coverage of reaction intermediates on active sites. Methanol can possibly be converted to other hydrocarbons during a long-term reaction, but in quantities that might be too low to be confirmed.

Oxygen is expected as a product of the CO₂ reduction (Eq. (1)). Fig. 12 shows that the time dependency of oxygen generation approximately matches that of the methanol yield. By and large, the ratio of methanol to oxygen is near constant, $\sim 3\text{--}1$. Free O₂ was suggested as being adsorbed on the surface of TiO₂ in the presence of water [14]. Consequently, the oxygen sensor detected only part of dissolved oxygen in these experiments. The O₂ evolution also plateaued after 16–18 h of reaction, revealing O₂ consumption by methanol re-oxidation.

NaOH solution was crucial in the photoreduction of CO₂ [19]. The methanol yield substantially increased with the addition of NaOH in our experiments, perhaps due to the following two reasons. First, the high concentration of OH[−] ions in aqueous solution could act as strong hole-scavengers and form OH radicals, thereby reducing the recombination of hole–electron pairs. The longer decay time of surface electrons would certainly facilitate the reduction of CO₂. Second, caustic NaOH solution dissolves more CO₂ than does pure water. The initial pH value of 0.2N NaOH solution was approximately 13.3, and decreased to nearly 7.3 after bubbling CO₂ in the reactor. Notably, photoreduction may have been accelerated by the high concentration of HCO₃[−].

The high yields of methanol can be obtained at the elevated CO₂ pressure of the reactor for the same reason. As shown in Fig. 13, the methanol yield clearly increased with the pressure of CO₂ up to 125 kPa, but decreased with further increases of pressure. Mizuno et al. also observed similar phenomena [20]. Higher molecular-weight hydrocarbons, such as ethanol, might be converted from methanol at higher CO₂ pressures. A trace of ethanol was detected in the reaction at the two higher pressures, but was too small to be quantified.

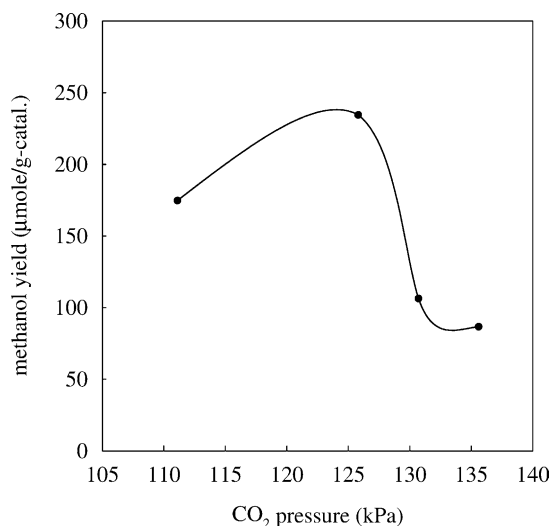


Fig. 13. Effect of CO₂ pressure on methanol yields at 6 h in 2.0 wt.% Cu/TiO₂.

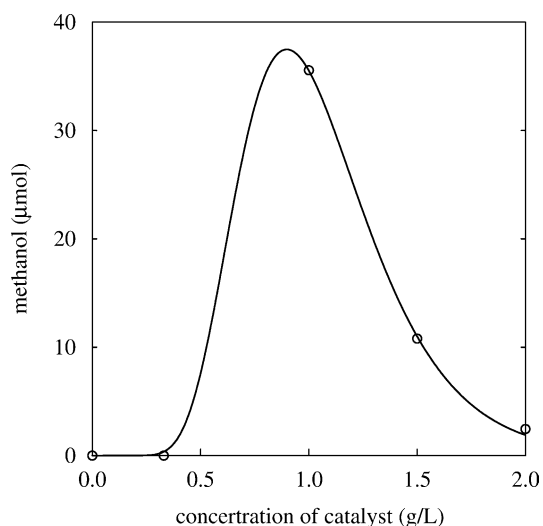


Fig. 14. Effect of catalyst charged (2.0 wt.% Cu/TiO₂) on methanol yield (CO₂ pressure: 125 kPa).

Fig. 14 shows that the methanol first increases then decreases with the amount of catalyst charged in the reactor. A higher concentration of catalyst is expected to correspond to greater absorption of UV energy, and thus a higher methanol yield. However, the yields of methanol begin to decline when the concentrations of catalyst exceed 1 g/l. The penetration

of UV light is cloaked in the reactor by the large quantity of catalyst in aqueous solution. The UV absorption of the outer catalyst is thus reduced, but the re-oxidation rate of methanol increases with the charge of the catalyst in the reactor. Consequently, the overall methanol yield decreases with excess catalyst.

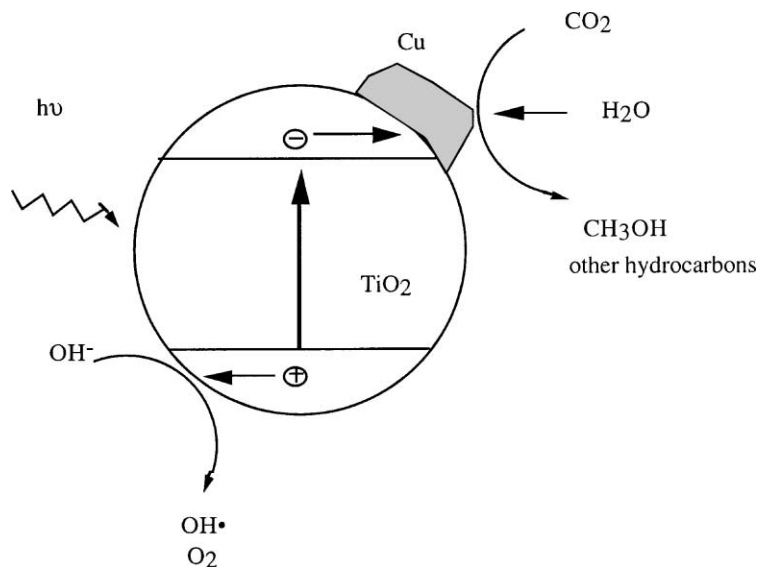


Fig. 15. Mechanism of CO₂ photocatalytic reduction on Cu/TiO₂.

3.3. Mechanism of the photocatalytic reduction of CO₂

Based on the above results, a photocatalytic mechanism is proposed and illustrated in Fig. 15 to describe the reduction of CO₂ with H₂O. Molecules of CO₂ (or HCO₃[−]) and H₂O interact with trapped electrons on the Cu cluster. The reduction of CO₂ and the decomposition of H₂O proceed competitively, and methanol is formed. The OH radicals are produced from OH[−] by scavenging holes on the TiO₂ surface, and these radicals may react with the carbon species formed from CO₂ to produce methanol. Free oxygen is also generated from the oxidation of OH[−] with holes, then can be partially consumed by the re-oxidation of methanol.

4. Conclusions

Methanol was favorably produced on TiO₂ and Cu/TiO₂ catalysts in a CO₂/NaOH aqueous solution under UV irradiation. Experimental results demonstrated that the homogeneous hydrolysis of titanium(IV) butoxide via the improved sol–gel route was a promising technique for preparing photocatalysts with uniform nanoparticles. An optimal Cu-loaded titania is a highly efficient photocatalyst for CO₂ reduction since copper is an effective electron trapper, able to reduce the recombination of electron–hole pairs. The OH[−] in aqueous solution is a powerful hole scavenger, enhancing the photocatalytic reactivity. Although the quantum and energy efficiencies so far are not much higher than those of natural photosynthesis in this study, the catalytic reduction of CO₂ has great advantage over green plants of not having to support a living system. Ideally, the transformation of photo to chemical energy by a non-living catalyst should be more efficient than that by a life-supporting one. The photocatalytic reduction of CO₂ is still in its infancy. There are still many opportunities for improvement. A highly efficient catalyst is the key to this field.

Acknowledgements

The authors would like to thank the China Petroleum Corporation and the National Science

Council of the Republic of China for financially supporting this research under contract no. NSC 87-CPC-E-002-007.

References

- [1] E.A. Laws, J.L. Berning, Photosynthetic efficiency optimization studies with the macroalga *Cracilaria tikvahiae*: implications for CO₂ emission control from power plants, *Bioresour. Technol.* 37 (1991) 25–33.
- [2] H. Yamashita, Y. Fujii, Y. Ichihashi, S.G. Zhang, K. Ikeue, D.R. Park, K. Koyano, T. Tatsumi, M. Anpo, Selective formation of CH₃OH in the photocatalytic reduction of CO₂ with H₂O on titanium oxides highly dispersed within zeolites and mesoporous molecular sieves, *Catal. Today* 45 (1998) 221–227.
- [3] S. Kuwabata, K. Nishida, R. Tsuda, H. Inoue, H. Yoneyama, Photochemical reduction of carbon dioxide to methanol using ZnS microcrystallite as a photocatalyst in the presence of methanol dehydrogenase, *J. Electrochem. Soc.* 141 (6) (1994) 1498–1503.
- [4] K. Hirano, K. Inoue, T. Yatsu, Photocatalysed reduction of CO₂ in aqueous TiO₂ suspension mixed with copper powder, *J. Photochem. Photobiol. A: Chem.* 64 (1992) 255–258.
- [5] J.C.-S. Wu, L.-C. Cheng, An improved synthesis of ultrafiltration zirconia membranes via the sol–gel route using alkoxide precursor, *J. Membr. Sci.* 167 (2) (2000) 253–261.
- [6] A.K. Bhattacharya, D.R. Pyke, R. Reynolds, G.S. Walker, C.R. Werrett, *J. Mater. Sci. Lett.* 16 (1997) 1–3.
- [7] H.-F. Chang, M.A. Saleque, W.-S. Hsu, W.-H. Lin, Effect of acidity and copper surface area of the Cu/Al₂O₃ catalyst prepared by electroless plating procedure on dehydrogenation reactions, *J. Mol. Catal.* 94 (1994) 233–242.
- [8] G.C. Chinen, C.M. Hay, H.D. Vandervell, K.C. Waugh, The measurement of copper surface areas by reactive frontal chromatography, *J. Catal.* 103 (1987) 79–86.
- [9] A.L. Linsebigler, G. Lu, J.T. Yates Jr., Photocatalysis on TiO₂ surface: principles, mechanisms, and selected results, *Chem. Rev.* 95 (1995) 735–758.
- [10] Z. Zhang, C.-C. Wang, R. Zakaria, J.Y. Ying, Role of particle size in nanocrystalline TiO₂-based photocatalysts, *J. Phys. Chem. B* 102 (1998) 10871–10878.
- [11] E. Sanchez, T. Lopez, Effect of the preparation method on the band gap of titania and platinum-titania sol–gel materials, *Mater. Lett.* 25 (1995) 271–273.
- [12] J.C. Vickerman, *Surface Analysis: The Principal Techniques*, Wiley, New York, 1997.
- [13] M. Halmann, in: M. Grätzel (Ed.), *Photochemical Fixation of Carbon Dioxide, Energy Resource Through Photochemistry and Catalysis*, Academic Press, New York, 1983 (Chapter 15).
- [14] H. Yamashita, H. Nishiguchi, N. Kamada, M. Anpo, Photocatalytic reduction of CO₂ with H₂O on TiO₂ and Cu/TiO₂ catalysts, *Res. Chem. Interme.* 20 (8) (1994) 825–833.

- [15] M. Anpo, T. Shima, S. Kodama, Y. Kubokawa, Photocatalytic hydrogenation of CH_3CCH with H_2O on small-particle TiO_2 : size quantization effects and reaction intermediates, *J. Phys. Chem.* 91 (1987) 4305–4310.
- [16] B.-J. Liu, T. Torimoto, H. Yoneyama, Photocatalytic reduction of CO_2 using surface-modified CdS photocatalysts in organic solvents, *J. Photochem. Photobiol. A: Chem.* 113 (1998) 93–97.
- [17] H. Inoue, H. Moriwaki, K. Maeda, H. Yoneyama, Photoreduction of carbon dioxide using chalcogenide semiconductor microcrystals, *J. Photochem. Photobiol. A: Chem.* 86 (1995) 191–196.
- [18] M. Scrocco, Satellite structure in the X-ray photoelectron spectra of CuO and Cu_2O , *Chem. Phys. Lett.* 63 (1) (1979) 52–56.
- [19] S. Kaneco, Y. Shimizu, K. Ohta, T. Mizuno, Photocatalytic reduction of high pressure carbon dioxide using TiO_2 powders with a positive hole scavenger, *J. Photochem. Photobiol. A: Chem.* 115 (1998) 223–226.
- [20] T. Mizuno, K. Adachi, K. Ohta, A. Saji, Effect of CO_2 pressure on photocatalytic reduction of CO_2 using TiO_2 in aqueous solutions, *J. Photochem. Photobiol. A: Chem.* 98 (1996) 87–90.